A study of the flow within shallow, narrow cavities at low Reynolds Numbers

Sarah Diane Crook

B.Eng (Mech., Hons.) and B.Sc (Physics)

A thesis submitted in fulfilment of the requirements for the degree of

Doctor of Philosophy, August 12, 2011

School of Mechanical Engineering

The University of Adelaide

South Australia 5005

Abstract

This thesis investigates low speed three-dimensional cavity flows. The flow past cavities, gaps and steps is of interest to researchers because these features are found on nearly all vehicles. Most past studies of cavity aerodynamics are of two-dimensional representations and although the literature provides valuable fundamental information on two-dimensional models and flow descriptions, they are inadequate when it comes to defining three-dimensional cavity flow.

The aim of this study is therefore to discover, by measurement and observation, the time-averaged three-dimensional structure of incompressible flow in an open rectangular cavity in a flat plate. Furthermore, the study will focus on asymmetries in the ensemble-averaged and transient flow.

The above aims are addressed by experimental investigation. Experimental data are obtained at low speed in both wind and water tunnels. The free stream Reynolds numbers are 3.4×10^5 in air and 4.3×10^4 in water. The ratio of cavity length (in the direction of the flow) to width to depth is $l{:}w{:}d$=6:2:1.

The first experiments are of flow visualisation in both a wind and water tunnel, followed by measurements of surface pressure in air. Lastly, the velocity field in and near the cavity is investigated using Particle Image Velocimetry (PIV) in water. The surface pressure data are presented as pressure coefficient distributions. PIV data are presented as two-component velocity vector fields and streamline patterns in cross sections of the cavity.

The experimental results show that a thin shear layer forms at the upstream lip of the cavity, and this grows and impinges on the downstream wall. The shear layer is subject to oscillations causing quazi-periodic mass flow addition and removal. Results show that close to the upstream cavity edge the shear layer maintains a laminar-like profile extending

downstream from the point of separation. The growth rate of the shear layer is determined and is characterised by the change in the vorticity thickness.

The time-averaged internal cavity flow patterns are in agreement with published observations of an open-type flow field. The flow was primarily characterised by a large region of flow recirculation. Experimental results show that a 6:2:1 cavity flow contains additional vortical features, all of which are three-dimensional in nature and more complex than previously reported. The locations and behaviors of the vortices have been identified, as have their role in transporting fluid throughout the cavity. Furthermore, the streamline images obtained from PIV data show that a strong asymmetry is present in the flow.

In general, the experimental data are topologically self consistent, although a number of anomalies and inconsistencies are identified. The inconsistencies between the flow features indicate that the asymmetry and oscillations are important features of the flow.

Two tornado vortices are present in the front region of the cavity and are responsible for transporting some of the reversed flow upwards into the shear layer. Their size and location are highly variable and asymmetric. The rotation sense of these tornado vortices for cavities with $l/d \geq 6$ is opposite to the rotation of tornado vortices reported within cavities with $l/d \leq 5$.

Conditionally-averaged PIV data are used to investigate the unsteady, asymmetric flow field. Two asymmetric fields and a symmetric field are identified and the streamline patterns and velocity distributions are mostly enantiomorphic. It is shown that the flow within the cavity is fundamentally unstable and asymmetric. The asymmetry appears to be the result of a twisting instability of the shear layer.

Declaration

This work contains no material which has been accepted for the award of any other degree or diploma in any university or other tertiary institution to Sarah Crook and, to the best of my knowledge and belief, contains no material previously published or written by another person, except where due reference has been made in the text.

I give consent to this copy of my thesis, when deposited in the University Library, being made available for loan and photocopying, subject to the provisions of the Copyright Act 1968.

I also give permission for the digital version of my thesis to be made available on the web, via the University's digital research repository, the Library catalogue and also through web search engines, unless permission has been granted by the University to restrict access for a period of time.

SIGNED:.....DATE:.....

Dedication

I would like to dedicate this thesis to my family.

My grandmother, Jean

My parents, Paul and Andrea

My brother and his wife, Ben and Maria

My loving partner, William

> "...and you learnt a lot you never knew before. And if the journey takes a lifetime when you thought a year or two, well you just don't give up easy anymore."

Slim

Acknowledgements

A number of people need to be thanked for their contribution to this research who make its completion possible.

Firstly, thanks go to my supervisors, Assoc. Prof. Richard Kelso and Dr. Peter Lanspeary; Prof. Kelso for his knowledge of fundamental fluid mechanics, particularly as an experimentalist, and Dr. Lanspeary for his involvement during the final crucial stages of this research.

Thanks are also given to Mr. Jan Drobik (Defence Science and Technology Organisation, DSTO) for his continued encouragement, support and providing access to facilities which would have been otherwise unavailable. Thanks also for the support of the DSTO for their sponsorship of the research and the scholarship provided.

I also thank the technical staff of the University of Adelaide Mechanical Engineering School. Specifically the Mechanical Engineering and Electronics Workshop for the advice and excellent craftsman-ship.

Particular mention and thanks must be given to my fellow researchers for their unconditional support and freely offered advice. Firstly I wish to acknowledge the enormous time and effort provided by Eyad Hassan during a crucial stage of this research. Eyad provided time, expertise, technical and moral support throughout all stages of PIV experiments from set-up to data analysis and advice thereafter. Thanks must also be given to a number of people for their moral support, encouragement and willingness to lend a hand: Tim Lau, Cris Birzer, Rebecca Jones, Susan Pearce, Billy Constantine, Tommie Liddy, Paul Medwell, and Michael Riese.

Thanks must also be given to Nova Systems for their continued encouragement and understanding during the final stages of my thesis writing.

Finally, special thanks and love to my parents, Andrea and Paul, my brother Ben and his wife Maria, for their encouragement. Last, but most importantly, I would like to thank Billy for his enduring patience, which was stretched numerous times, loving support and financial help throughout the last few years of my candidature. His support ensured that completion of this thesis was easier than it otherwise might have been, and for this I am extremely grateful.

Sarah Diane CROOK

August 12, 2011

Contents

List of Figures

List of Tables

Abbreviations

2D	Two dimensional
3D	Three dimensional
BFS	Backward facing step
CCD	Charged coupled device
CFD	Computational fluid mechanics
CR4	Fourth-order, hybrid, compact-Richardson extrapolation
CW	Clockwise
CCW	Counter-clockwise
DLR	Deuttsches Zentrum für Luft-und Raumfahrt (German Aerospace Centre)
DSTO	Defence Science and Technology Organisation (Australia)
KAO	Kuiper Airborne Observatory
LES	Large-eddy simulation
LDV	Laser-doppler velocimetry
MDF	Medium density fibreboard
NASA	National Aeronautics and Space Administration
Nd:YAG	Neodymium-doped yttrium aluminium garnet
PIV	Particle image velocimetry
rms	Root mean squared
RANS	Reynolds-averaged numerical simulation
SOFIA	Stratospheric Observatory for Infrared Astronomy
SPL	Sound pressure levels

List of Symbols

A_c	Cavity reference area, depth × width
$\frac{a}{b}$	Geometric parameter defining the slenderness of a super-elliptic profile
α	Angle of attack; phase lag
C	Centroid
c	Speed of sound
C_d	Drag coefficient, $C_d = \frac{D}{q.A_c}$
C_p	Pressure coefficient, $C_p = \frac{p_x - p_o}{q}$
d	Pitot probe diameter
d^*	non-dimensional Pitot probe diameter, $\frac{dU_\tau}{\mu}$
dB	Decibel
dB(A)	A-weighted decibel
ρ	Density
d	Depth of cavity
D	Drag force
δ	Boundary-layer thickness
δ_w	Pitot probe proximity correction shift
f	Frequency of instability wave;
	frequency of fluid velocity or pressure fluctuation; resonance frequency
f_{ac}	Frequency of radiated sound
κ	Normalised convection velocity $\frac{U_c}{U_\infty}$
h	Height of the cavity or step
H	Shape factor, $\frac{\delta^*}{\theta}$
l	Length of cavity
l/d	Length-to-depth ratio of cavity
l/d_{cr}	Critical length-to-depth ratio
L	Boundary-layer development length
L_r	Ruler length used for PIV calibration
λ_{ac}	Acoustic wavelength

M	Mach number, U/c
M_1	First moment
m	Stage number; number of wavelength of instability waves in the shear layer at any instant in time (also refers to the dominant oscillation state, typically 1, 2, 3 or 4)
$\dot{m}$	Met mass flow
N	Number of samples; number of PIV image pairs
p_o	Free-stream static pressure
p_x	Surface pressure at location $\vec{x}$ (location is defined by x, y and z)
P_{rms}	Root-mean-square of the pressure signal
P_e	Pressure in the local shear layer
q	Free-stream dynamic pressure, $\frac{1}{2}\rho U_\infty^2$
Re_l	Reynolds number based on length l
Re_d	Reynolds number based on depth d
Re_δ	Reynolds number based on boundary-layer thickness δ
$Re_\delta*$	Reynolds number based on displacement thickness $\delta*$
Re_θ	Reynolds number based on boundary-layer thickness θ
r or r_o	PIV conversion factor (m/pixel)
$\vec{s}$ or $\overline{\lvert\langle\vec{s}\rangle\rvert}$	PIV mean particle displacement (pixels)
St	Strouhal number
Δt	PIV time delay between two images
τ	Wall shear stress
ν	Kinematic Viscosity
μ	Dynamic Viscosity
σ and ε	Uncertainty in the data
ε_{Ub}	Bias uncertainty in the mean velocity
ε_{Ut}	Random error / turbulence component of uncertainty in the mean velocity
σ_r	Uncertainty in the PIV conversion factor
σ_s	Uncertainty in the PIV particle displacement
σ_t	Uncertainty in the PIV time delay, also known as jitter of the laser pulse
$\frac{\sigma_x}{\Delta X}$	Relative uncertainty in the data
$\frac{\sigma_t}{\Delta t}$	PIV error: pulse separation rms jitter / pulse separation
$\frac{\sigma_r}{\Delta L}$	PIV error: uncertainty in length calibration / length calibrated
$\frac{\sigma_d}{\Delta D}$	PIV error: uncertainty in particle image diameter / particle displacement
$\frac{\sigma_D}{\Delta D}$	PIV error: uncertainty in particle image displacement / particle displacement
$\frac{\sigma_\rho}{\Delta \rho}$	PIV error: uncertainty in particle image density / particle displacement
$\frac{\sigma_q}{\Delta D}$	PIV error: uncertainty in image quantization / particle displacement
$\frac{\sigma_n}{\Delta D}$	PIV error: uncertainty in noise / particle displacement
$\frac{\sigma_{\Delta V}}{\Delta D}$	PIV error: uncertainty in velocity gradient / particle displacement

θ	Momentum thickness
U_∞	Mean free-stream velocity
$\vec{U}$	PIV velocity vector, $\frac{r.\vec{s}}{\Delta t}$
U_c	Convection velocity of instabilities in the shear layer
U_l	Velocity in shear layer lower stream
U_u	Velocity in the shear layer upper stream
U_e	Velocity in the local shear layer
U_τ	Friction velocity, $\sqrt{\tau/\rho}$
u, v, w	Instantaneous velocity at a point (x-, y- and z-component)
$\overline{u}$, $\overline{v}$, $\overline{w}$	Mean velocity at a point (x-, y- and z-component)
u', v', w'	Instantaneous velocity fluctuations at a point (x-, y- and z-component)
$\overline{u}'$, $\overline{v}'$, $\overline{w}'$	Mean velocity fluctuations at a point (x-, y- and z-component)
$\overline{\lvert\langle\vec{U}\rangle\rvert}$, $\overline{\lvert\langle\vec{V}\rangle\rvert}$, $\overline{\lvert\langle\vec{W}\rangle\rvert}$	Mean velocity, also expressed as U, V and W (x-, y- and z-component)
w or w_c	Width of cavity
w/d	Width-to-depth ratio of cavity
ω	Vorticity
δ_ω	Vorticity thickness
x	x coordinate (lengthwise direction); distance from front wall of cavity
y	y coordinate (depthwise direction); distance from the surface of the support plate
Δy	Shift in y position
z	z coordinate (spanwise direction)
ζ	Blasius similarity variable, $\frac{y}{2}\sqrt{\frac{U_\infty}{(x+L)\nu}}$

Cavity Parameters and Coordinate System

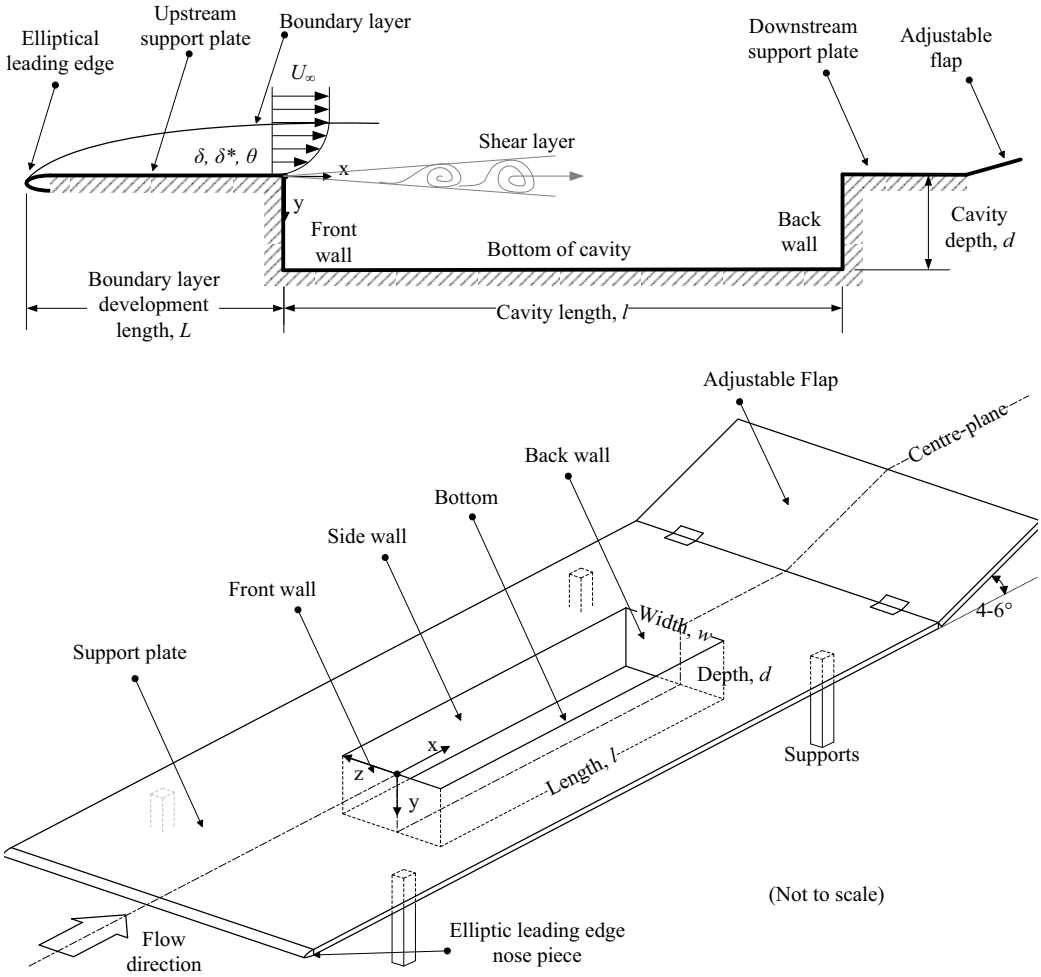

Commonly used cavity parameters for wind and water tunnel experiments			
Symbol	Description	Value in air	Value in water
l	Length of cavity	450mm	450mm
d	Depth of cavity	75mm	75mm
w	Width of cavity	150mm	150mm
$l:d:w$	length : depth : width ratio	6:1:2	6:1:2
L	Boundary layer development length	465mm	360mm
U_∞	Free stream velocity	10.6m/s	106mm/s
δ	Boundary layer thickness	12.2mm	11.2mm
δ^*	Displacement thickness	2.1mm	3.2mm
θ	Momentum thickness	1.5mm	1.2mm
	Boundary-layer type	turbulent	laminar
Re_l	Reynolds number based on l	3.4×10^5	4.3×10^4
Re_d	Reynolds number based on d	5.4×10^4	0.7×10^4
Re_δ	Reynolds number based on δ	8,790	1,050
Re_{δ^*}	Reynolds number based on δ^*	1,519	326
Re_θ	Reynolds number based on θ	1,078	138